Editors' Suggestion

Carrier Mobility up to 10^6 cm^2 V^{-1} s^{-1} Measured in Single-Crystal Diamond by the Time-of-Flight Electron-Beam-Induced-Current Technique

A. Portier,[1,2,*] F. Donatini,[2] D. Dauvergne,[1] M.-L. Gallin-Martel,[1] and J. Pernot[2,†]

[1] *Université Grenoble Alpes, CNRS, Grenoble INP, LPSC-IN2P3, Grenoble 38000, France*

[2] *Université Grenoble Alpes, CNRS, Grenoble INP, Institut Néel, Grenoble 38000, France*

(Received 20 January 2023; revised 2 May 2023; accepted 24 July 2023; published 16 August 2023)

Diamond is a very promising material for various applications, and understanding its basic properties is key for the development of future devices. In particular, the low-field mobility of holes has never been measured below ∼ 80 K in ultrapure diamond. In order to measure this mobility, we developed an innovative time-of-flight electron-beam-induced-current technique. A 1 ns pulsed electron beam was made to impact the diamond semiconductor, inducing charge-carrier creation and motion through the 546-μm-thick bulk diamond, under the influence of an applied electric field. The resulting signal was analyzed using the transient-time technique. Thus, the velocity of electrons and holes was assessed as a function of the temperature from 13 to 300 K and as a function of the electric field with values ranging from 1.5 to 9200 V cm^{-1}. A low-field mobility value of $1.03 \pm 0.05 \times 10^6$ cm^2 V^{-1} s^{-1} was measured for holes at 13 K, demonstrating that diamond is a suitable material to transport charge carriers in a ballistic regime at a scale of 10 μm.

DOI: 10.1103/PhysRevApplied.20.024037

I. INTRODUCTION

Single-crystal diamond is a fascinating material because of its ultrawide band gap, large breakdown field, radiation hardness, and excellent charge transport properties. These properties mean diamond can be used in varying fields, including particle detection [1], power electronics [2], "valleytronics" [3,4], and so forth. Among diamond's aforementioned properties, charge-carrier mobility is perhaps the most relevant property for many applications. The electron and hole mobilities in ultrapure diamond have been thoroughly investigated over the last four decades by different time-of-flight (TOF) techniques [3,5–15], also called transient-current techniques (TCT), and by time-resolved cyclotron resonance (TRCR) [16,17] and continuous-wave cyclotron resonance (CWCR) [18].

Very high electron mobility was reported by both TCT [15] and cyclotron resonance techniques [16–18]. Recent CWCR experiments enabled researchers to assess electron mobility values up to 100×10^6 cm^2 V^{-1} s^{-1} at 3 K [18], which is 16 times higher than previously reported TRCR values. However, the low-field mobility of holes has never been measured in ultrapure material by TCT, at temperatures below ∼ 80 K. Although some previous studies have reported a saturation of the hole low-field mobility of around 10^4 cm^2 V^{-1} s^{-1} at 2 K because of neutral impurities within the crystal [14], other experiments found that it is necessary to reach extremely low electric fields to perform these measurements below ∼ 80 K in ultrapure diamond [13]. As a result, the highest hole low-field mobility reported using TCT is between 1×10^4 and 2×10^4 cm^2 V^{-1} s^{-1} [6,11] at about 80 K. Using the TRCR technique, hole drift low-field mobility values of 2.3×10^6 cm^2 V^{-1} s^{-1} for light holes and 2.4×10^5 cm^2 V^{-1} s^{-1} for heavy holes at 10 K were measured in 2014 [16].

These mobility values allow us to consider mean free paths of more than 10 μm, which are particularly important for the realization of large-scale quantum devices requiring coherent and thus ballistic transport between distant qubits, i.e., color centers in diamond [19,20]. However, these mobility values were determined by using the momentum scattering time assessed from the cyclotron resonance linewidth in a region delineated by the cyclotron radius of the measured carriers. In this context, a large-scale distance measurement, as achieved through drift velocities by TOF techniques where the carriers pass through the entire thickness of a several-hundred-micrometers thick sample, is necessary to demonstrate the possibility of achieving large-scale ballistic transport.

In the various TOF measurements, different particles were used in order to generate electron-hole pairs just below an electrode, such as α particles [1,8,10,14,21,22], pulsed x rays [23], UV light [3,11–13], and accelerated

*alexandre.portier@lpsc.in2p3.fr

†julien.pernot@neel.cnrs.fr

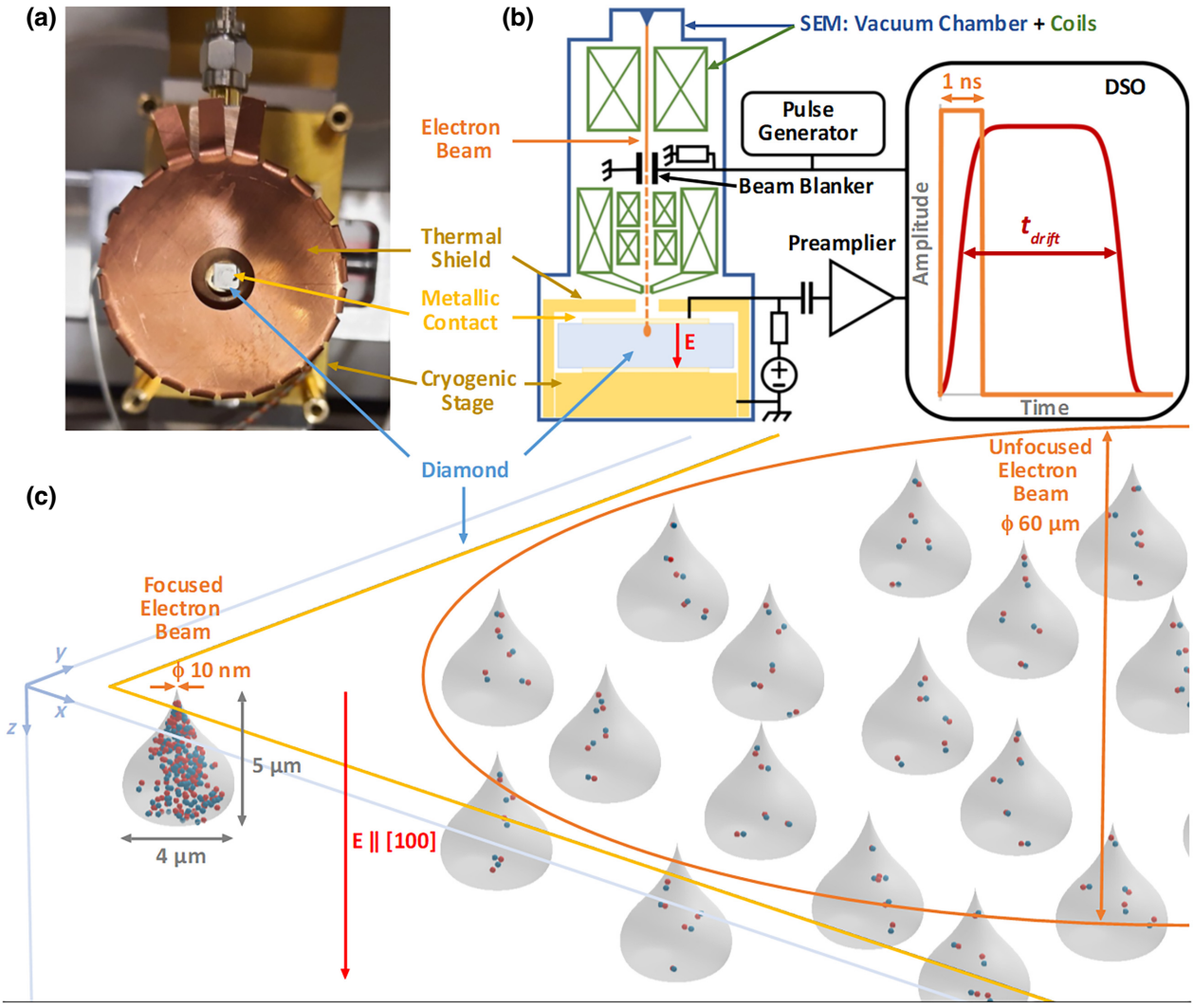

FIG. 1. Time-of-flight electron-beam-induced-current setup. (a) Top view of the diamond sample on the cryogenic stage surrounded by the copper thermal shield. (b) Schematic of the electron-beam set up, the signal conditioning, and the digital storage oscilloscope (DSO) treatment. The orange curve of the chronogram corresponds to the electron-beam current pulse controlled by the beam blanker. The red curve corresponds to the current passing through the diamond, induced by the applied electric field E, and processed by the preamplifier. (c) Schematic of the electron-hole pair (respectively the blue and red dots) populations created within a focused electron beam and an unfocused electron beam. The orange line delineates the lateral size of the unfocused beam and the yellow line the outer limit of the metallic contact through which the beam excites the electron-hole pairs in diamond. The gray pear-shaped volumes represent the random lateral distribution of the regions, where the electron-hole pairs may be created by each primary electron impacting the sample surface.

pulsed electrons [6,24]. Then the current induced by the drift of one type of charge carrier under an applied electric field was measured as a function of time. The other type of carrier was collected almost immediately. This phenomenon can be described by the Shockley-Ramo theorem [25,26].

In this work, we propose a low-temperature time-of-flight technique using a pulsed electron beam to generate carriers, which induce a current under an applied electric field—called the time-of-flight electron-beam-induced-current (TOF-EBIC) technique. A similar experiment was developed by Quaranta *et al.* [24] and used to study hole transport properties at various temperatures [6]. Our TOF-EBIC technique allowed us to monitor multiple properties independently and simultaneously. (1) Our experiment determined the in-depth distribution of electron-hole pairs close to the contact by varying the energy of the electron beam from 500 eV to 30 keV (penetration depth up to ~ 5 µm). (2) Our experiment monitored the electron-hole pairs generated at different electron-beam currents ranging from 4 pA to 100 nA during the pulse. (3) Our method examined the lateral distribution of charge carriers

within a pulse and during all the acquisition time through the focus and the deterministic positioning of the beam, respectively. Thanks to this added freedom and our use of a careful method to avoid the polarization effect in high-quality and ultrapure diamond, we successfully measured the low-temperature velocity for electric fields as low as 1.5 V cm^{-1} for holes and 18 V cm^{-1} for electrons.

The first section of this report describes the experimental setup and the originality of the method. The second section analyzes the TOF-EBIC traces of electrons and holes, and assesses the drift velocity versus electric field and temperature. Then, the low-field mobility values of both carriers are reported versus temperature, demonstrating that values up to 10^6 cm^2 V^{-1} s^{-1} were achieved in the case of holes.

II. EXPERIMENTAL DETAILS AND METHOD

A (546 ± 4)-μm-thick single-crystal diamond, grown through chemical vapor deposition (SCCVD) and with an electronic-grade quality ([N] $< 9 \times 10^{14}$ cm^{-3}, typically (0.2–2) $\times 10^{14}$ cm^{-3}, and [B] $< 2 \times 10^{14}$ cm^{-3}) from Element Six has been investigated. The bottom and upper sides of the diamond were metallized using laser lithography and vapor deposition systems. The metallization was composed of a 10/100 nm bilayer of titanium/aluminum.

The TOF-EBIC setup proposed here [Figs. 1(a) and 1(b)] is based on the architecture of a scanning electron microscope (SEM). The SEM was an FEI Inspect F50 fitted with an in-house beam blanker driven by a 70-ps rise- and fall-time pulse generator (Pulse Rider PG-1072 from Active Technologies). The pulses of electrons are generated with a full width at half maximum of 1 ns at a frequency of 333 Hz. The sample was biased using voltage values ranging from −500 to 500 V. The readout system was composed of one CIVIDEC C2HV current preamplifier with a 2-GHz bandwidth connected to a 40-GSa (gigasamples per second) digital sampling oscilloscope (DSO; LeCroy HDO 9404). It was possible to cool the sample to 13 K with a liquid-helium cryogenic stage (Gatan CF302) equipped with a thermal shield. Silver paste was used to attach the bottom side of the diamond to the cryogenic stage (side electrically grounded) and to connect a thermalized cable on its upper side. To obtain an accurate and real-time reading of the temperature of the sample, a calibrated CERNOX sensor (CX-1070-S-HT-4L) was mounted close to the diamond.

To obtain a high signal-to-noise ratio, the electron-beam energy was set at 30 keV to generate a charge of about 11 fC per pulse in the diamond device. During the 1-ns electron-beam pulse, around 30 primary electrons collided with the diamond surface covered with a 110-nm-thick Ti/Al contact layer. A 33-ps average time separated each primary electron impact, which generated an average of 2200 electron-hole pairs during the electron-matter interaction within a time frame less than 1 ps, in a pear-shaped volume 5 μm deep and 4 μm wide [see Fig. 1(c)].

However, to avoid local effects especially at a low applied electric field (i.e., when electrons and holes generated during consecutive impacts mixed together because of their low drift velocities), the primary electron beam was unfocused to form a spot of 60 μm diameter [see Fig. 1(c)]. Under these conditions, each primary electron of a single pulse interacted in its own pristine volume, free of charges from previous impacts. This allowed us to minimize polarization effects, i.e., internal electric field induced by the trapping of charge carriers, and carrier-carrier interactions, i.e., electron-hole recombination rate and local electric field screening.

Moreover, after a high-energy irradiation, a mixture of excitons and free carriers is generated. Because of the large binding energy of excitons in diamond, the fraction of excitons of the mixture at equilibrium is almost equal to 1 at low temperatures [27]. Conversely to free charge carriers, the excitons are neutral particles and thus are not impacted by the electric field, which could lead us to conclude that the TOF-EBIC technique cannot be used at low temperatures. Nevertheless, by applying an electric field, the electrons and the holes drift in opposite directions and can thus be separated prior to the formation of excitons. This effect is limited when the excitation density is high [around 10 nm focused electron beam in Fig. 1(c)] due to the difficulty of separating the charge carriers in a large and dense cloud of electrons and holes. Again, conversely, for low carrier density [unfocused electron beam in Fig. 1(c)], this phenomenon is sufficient to decrease the quantity of excitons generated significantly.

III. TEMPERATURE DEPENDENCE OF THE DRIFT VELOCITY AND CARRIER MOBILITY

The TOF-EBIC traces shown in Fig. 2 were obtained by averaging single waveforms taken at different positions as the beam was scanned over an area, allowing the spatial separation of pulses (typically 200 μm apart). Once the area was scanned, the acquisition was paused and then, to reset the state of the diamond, a cycling procedure was performed by inverting the bias polarity for 1 s while keeping the electron-beam excitation constant. Finally, the acquisition process was resumed. The acquisition and cycling procedures could be repeated 100 times for the lower electric fields to obtain waveforms in which the rising and falling edges of the signal could be clearly identified.

These traces for electrons and holes were obtained at different temperatures and different applied electric fields. Multiple conclusions can be drawn from these results. First, the transit times are systematically shorter for holes than for electrons, across all the electric fields and temperatures. Secondly, the transit time of both carriers increases

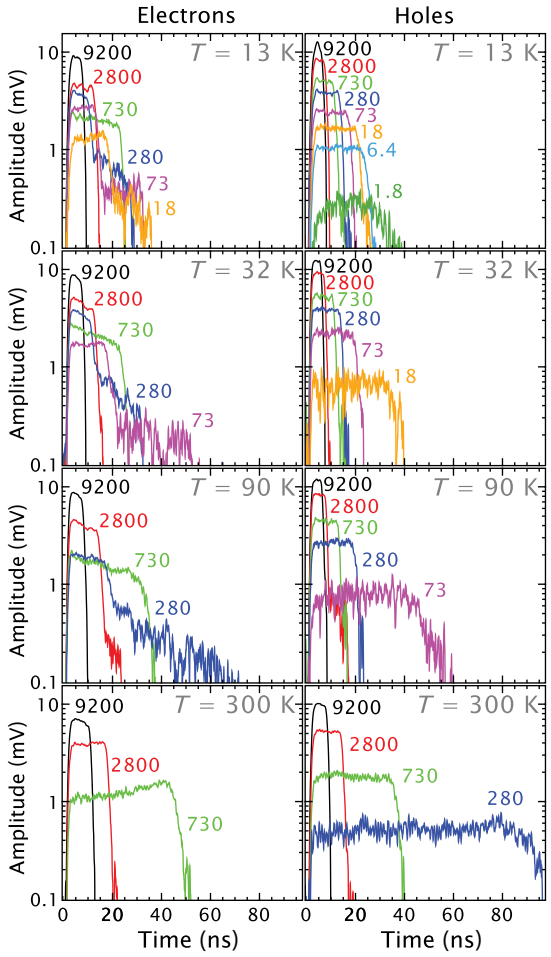

FIG. 2. Time-of-flight traces of electrons and holes, measured at different temperatures ($T = 13,\ 32,\ 90$, and 300 K) and electric fields. The electric field ($\mathrm{V\,cm^{-1}}$) is specified in a label in a corresponding color next to each curve.

with the temperature for a given electric field (except for the electron transits measured at 120 and 150 K), demonstrating that the drift velocity decreases with temperature [see also Figs. 3(a)–3(d)] with a maximum value measured at 13 K for a given electric field. For temperatures above 150 K, the signal shapes of electrons and holes are very similar. However, for temperatures below 150 K and for low electric fields ($E < 500\ \mathrm{V\,cm^{-1}}$), the electron signal differs fundamentally from the signal of holes, with traces accounting for two steps. Indeed, for these traces, the transits of the electrons in the longitudinal (cool electrons) and transverse (hot electrons) valleys can be studied separately. The first contribution of the signal was attributed to the hot electrons, which have a lower effective mass than the cool electrons [29]. Valley-polarized electrons were experimentally observed in diamond samples and theoretically described by Isberg *et al.* [3] in 2013.

To estimate the drift velocity, the method described by Isberg *et al.* [30–32] (see also Ref. [33]) was used to reproduce $I(t)$, the amplitude of the trace versus time of Fig. 2, and extract its full width at half maximum as well as the experimental uncertainties [34]. In Figs. 3(a)–3(d), the drift velocities of holes and electrons versus the electric field are shown for temperatures between 13 and 300 K. For most cases, it is remarkable that an ohmic behavior was observed at the lowest electric field and thus that the low-field mobility μ_0 values could be extracted by a linear fit (solid lines).

The hole and electron low-field mobilities were estimated as $2190 \pm 30\ \mathrm{cm^2\,V^{-1}\,s^{-1}}$ and $1660 \pm 10\ \mathrm{cm^2\,V^{-1}\,s^{-1}}$, respectively, at room temperature. These values are consistent with the low-field mobilities, measured using TCT, reported in the literature [1,10,11,21,23]. Figure 3(c) shows that, at 120 K, the electron drift velocity decreases between 360 and 550 $\mathrm{V\,cm^{-1}}$. This phenomenon is called negative differential mobility and it was observed for the first time in a diamond sample by Isberg *et al.* [12] in 2012. Our measurements accurately reproduce their results obtained at 120 K, which demonstrates the reliability of our method. For temperatures greater than 220 K [Figs. 3(c) and 3(d)], a fit within the whole electric field range was also performed using Eq. (1) (dashed line) [35]:

$$v_{\mathrm{drift}}(E) = \frac{\mu_0 E}{1 + (\mu_0 E / v_{\mathrm{sat}})}, \tag{1}$$

where v_{drift} is the drift velocity, E the applied electric field, μ_0 the low-field mobility, and v_{sat} the saturation drift velocity. This fit function accurately describes the electric field dependence of the drift velocity at high temperatures (higher than ~ 200 K).

The established empirical model described by Caughey and Thomas [35] cannot be used for holes at the lowest temperatures as reported by Majdi *et al.* [13]. Indeed, at low temperatures, the accelerating electric field leads to the carrier temperature becoming substantially larger than the lattice temperature, inducing a deviation from the ohmic behavior. As expected, the threshold of the electric field delineating the ohmic behavior to the hot-carrier behavior increases with temperature. Very low fields are needed to assess the mobility values at low temperature (see Ref. [36]). For example, electric fields lower than 10 $\mathrm{V\,cm^{-1}}$ are needed for temperatures lower than 30 K. Our optimized experimental method enabled us to maximize the signal-to-noise ratio and thus measure the TOF-EBIC signals at extremely low fields reaching the ohmic region.

The temperature dependence of the low-field mobility of electrons and holes is shown in Fig. 3(e). It is important to note the extremely high mobility value of holes measured in this work, $\mu_0 = (1.03 \pm 0.05) \times 10^6\ \mathrm{cm^2\,V^{-1}\,s^{-1}}$ at 13 K. This mobility can be compared with the hole mobility value of $6.4 \times 10^5\ \mathrm{cm^2\,V^{-1}\,s^{-1}}$ averaged from

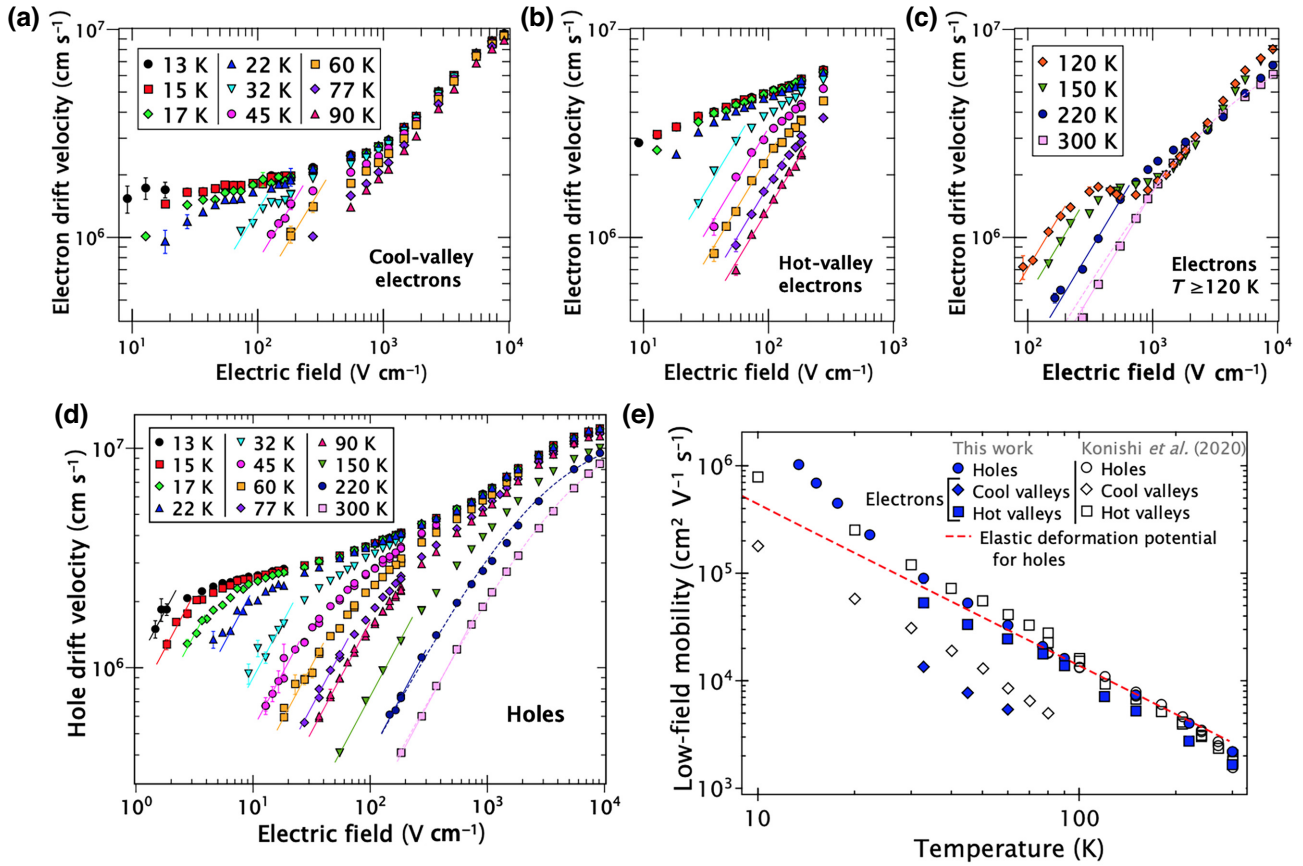

FIG. 3. Electron and hole drift velocities and low-field mobilities. (a) Cool-valley and (b) hot-valley electron drift velocity versus electric field at various temperatures. The temperatures in panel (b) are indicated in the legend in panel (a). (c) Electron drift velocity versus electric field measured above 120 K. (d) Hole drift velocity versus electric field at various temperatures. The solid lines show the linear fit at low electric fields used to extract the low-field mobility. A fit on the entire electric field range was also performed using Eq. (1) at 220 and 300 K (dashed lines). (e) Hole and electron low-field mobility versus temperature. The filled blue markers correspond to the values extracted during this work and the open markers to the value of Konishi *et al.* [17]. The red dashed line represents the theoretical low-field mobility expected for holes based only on the elastic deformation potential extracted from Pernot *et al.* [28].

the light- and heavy-hole mobility values (2.3×10^6 and 2.4×10^5 cm^2 V^{-1} s^{-1}, respectively) at 10 K from Akimoto *et al.* [16]. Considering the heavy- and light-hole bands separately (see Ref. [37]), the light-hole mobility $\mu_{lh} \cong 3.62 \times 10^6$ cm^2 V^{-1} s^{-1} and heavy-hole mobility $\mu_{hh} \cong 3.88 \times 10^5$ cm^2 V^{-1} s^{-1} values have been evaluated from this work.

The average mobility value measured in the present work is the highest value reported for holes in a bulk semiconductor, approaching the hole mobility of two-dimensional GaAs systems, 5.8×10^6 cm^2 V^{-1} s^{-1}, measured at 0.3 K [38], or graphene, 1.4×10^6 cm^2 V^{-1} s^{-1}, measured at 1.8 K [39].

The hole mobility values reported here are also higher than those of electrons in diamond measured by UV TOF [17] as shown in Fig. 3(e). However, Konishi *et al.* [18] recently reported electron mobility values of up to 100×10^6 cm^2 V^{-1} s^{-1} measured by CWCR, a local probe technique, at 3 K. Mobility values measured by cyclotron resonance have been explained to be higher than macroscopic measurements due to crystalline inhomogeneity [17].

For temperatures higher than $T = 30$ K, a $T^{-3/2}$ mobility dependence was observed. This dependence was expected because of the acoustic-phonon scattering of holes, which is the main limitation for ultrapure material in this temperature range. Calculations were performed to evaluate the hole low-field mobility at low temperatures [28], and the theoretical results were compared to the experimental data. It is important to note that the theoretical hole low-field mobility thus calculated does not take into account the inelastic acoustic-phonon scattering of holes. As a result, for $T < 30$ K, a discrepancy between the elastic model and the experimental data could be observed. Indeed, the inelastic scattering phenomenon leads to higher hole low-field mobility. Therefore, if the crystal can be considered sufficiently pure to the extent that the elastic scattering caused by impurities can be neglected, hole low-field

mobility values comparable to those measured for electrons (100×10^6 cm^2 V^{-1} s^{-1} at 3 K [18]) are expected at a temperature of a few kelvins. In any case, the light- and heavy-hole mobility values extracted here correspond to a relaxation time of $\tau_{lh} \cong 537$ ps and $\tau_{hh} \cong 146$ ps and mean free paths of $l_{lh} \cong 25$ μm and $l_{hh} \cong 4.3$ μm (see Ref. [37]). The mean free path of light holes is around 20 times shorter than the 546-μm gap between electrodes, meaning that the transport regime is quasiballistic for such carriers.

The hole mean free path larger than 10 μm at a macroscopic scale above liquid-helium temperature ($T = 4$ K) provides new opportunities to transport quantum information and preserve its coherence between two qubits in diamond. Recently, Lozovoi *et al.* [19] proposed a method based on confocal fluorescence microscopy and magnetic resonance to induce and probe charge transport between individual nitrogen-vacancy centers in diamond at room temperature. The same group argued that the use of an external electric field and the lowering of temperature should drastically improve the hole transport fidelity due to a ballistic regime on a scale comparable with the inter-qubit distance [20]. Our work demonstrates the possibility of reaching ballistic regime at this scale and provides accurate data concerning the achievable distance-temperature tradeoff needed to increase the transport fidelity.

IV. SUMMARY

In summary, thanks to the implementation in an SEM of a time-of-flight technique based on electron pulses to generate carriers in bulk diamond, we were able to measure the electron and hole drift velocities from the transient currents down to 13 K for a large range of electric field (1.5 to 9200 V cm^{-1}). The low-field mobility of the charge carriers was extracted and compared with the literature. At 13 K, the low-field mobility of holes was found to reach a remarkable value of $1.03 \pm 0.05 \times 10^6$ cm^2 V^{-1} s^{-}1. This value corresponds to the highest averaged hole low-field mobility measured in a bulk semiconductor.

ACKNOWLEDGMENTS

This work is supported by IDEX Université Grenoble Alpes. The authors are grateful to Philippe Bergonzo (SEKI Diamond, USA) for fruitful discussions; to Christophe Hoarau, as well as all the electronics and instrumentation detector department teams from LPSC (CNRS, France), for the electronics development; and to the Nanofab team of Institut Néel for the clean-room process.

[1] C. Canali, E. Gatti, S. F. Kozlov, P. F. Manfredi, C. Manfredotti, F. Nava, and A. Quirini, Electrical properties and performances of natural diamond nuclear radiation detectors, Nucl. Instrum. Methods **160**, 73 (1979).

[2] N. Donato, N. Rouger, J. Pernot, G. Longobardi, and F. Udrea, Diamond power devices: State of the art, modelling, figures of merit and future perspective, J. Appl. Phys. **53**, 093001 (2019).

[3] Jan Isberg, Markus Gabrysch, Johan Hammersberg, Saman Majdi, Kiran Kumar Kovi, and Daniel J. Twitchen, Generation, transport and detection of valley-polarized electrons in diamond, Nat. Mater. **12**, 760 (2013).

[4] N. Suntornwipat, S. Majdi, M. Gabrysch, K. K. Kovi, V. Djurberg, I. Friel, D. J. Twitchen, and J. Isberg, A valleytronic diamond transistor: Electrostatic control of valley currents and charge-state manipulation of NV centers, Nano Lett. **21**, 868 (2021).

[5] F. Nava, C Canali, C Jacoboni, and L Reggiani, Electron effective masses and lattice scattering in natural diamond, Solid State Commun. **33**, 475 (1980).

[6] L. Reggiani, S. Bosi, C. Canali, F. Nava, and S. F. Kozlov, Hole-drift velocity in natural diamond, Phys. Rev. B **23**, 3050 (1981).

[7] Jan Isberg, Johan Hammersberg, Erik Johansson, Tobias Wikström, Daniel J. Twitchen, Andrew J. Whitehead, Steven E. Coe, and Geoffrey A. Scarsbrook, High carrier mobility in single-crystal plasma-deposited diamond, Science **297**, 1670 (2002).

[8] M. Pomorski, E. Berdermann, A. Caragheorgheopol, M. Ciobanu, M. Kiš, A. Martemiyanov, C. Nebel, and P. Moritz, Development of single-crystal CVD-diamond detectors for spectroscopy and timing, Phys. Stat. Sol. (a) **203**, 3152 (2006).

[9] Nicolas Tranchant, Dominique Tromson, Philippe Bergonzo, and Milos Nesladek, Single crystal CVD diamond growth for detection device fabrication, MRS Proc. **1039**, 1039–P10–03 (2007).

[10] Miloš Nesladek, Anna Bogdan, Wim Deferme, Nicolas Tranchant, and Philippe Bergonzo, Charge transport in high mobility single crystal diamond, Diam. Relat. Mater. **17**, 1235 (2008).

[11] Markus Gabrysch, Saman Majdi, Daniel J. Twitchen, and Jan Isberg, Electron and hole drift velocity in chemical vapor deposition diamond, J. Appl. Phys. **109**, 063719 (2011).

[12] J. Isberg, M. Gabrysch, S. Majdi, and D. J. Twitchen, Negative electron mobility in diamond, Appl. Phys. Lett. **100**, 172103 (2012).

[13] S. Majdi, K. K. Kovi, J. Hammersberg, and J. Isberg, Hole transport in single crystal synthetic diamond at low temperatures, Appl. Phys. Lett. **102**, 152113 (2013).

[14] Hendrik Jansen, Daniel Dobos, Thomas Eisel, Heinz Pernegger, Vladimir Eremin, and Norbert Wermes, Temperature dependence of charge carrier mobility in single-crystal chemical vapour deposition diamond, J. Appl. Phys. **113**, 173706 (2013).

[15] S. Majdi, M. Gabrysch, K. K. Kovi, N. Suntornwipat, I. Friel, and J. Isberg, Low temperature conduction-band transport in diamond, Appl. Phys. Lett. **109**, 162106 (2016).

[16] Ikuko Akimoto, Yushi Handa, Katsuyuki Fukai, and Nobuko Naka, High carrier mobility in ultrapure diamond

measured by time-resolved cyclotron resonance, Appl. Phys. Lett. **105**, 032102 (2014).
[17] K. Konishi, I. Akimoto, H. Matsuoka, V. Djurberg, S. Majdi, J. Isberg, and N. Naka, Low-temperature mobility-lifetime product in synthetic diamond, Appl. Phys. Lett. **117**, 212102 (2020).
[18] K. Konishi, I. Akimoto, H. Matsuoka, J. Isberg, and N. Naka, Intrinsic Mobility of Low-Density Electrons in Photoexcited Diamond, Phys. Rev. Appl. **17**, L031001 (2022).
[19] A. Lozovoi, H. Jayakumar, D Daw, G. Vizkelethy, E. Bielejec, Marcus W. Doherty, J. Flick, and C. A. Meriles, Optical activation and detection of charge transport between individual colour centres in diamond, Nat. Electron. **4**, 717 (2021).
[20] Artur Lozovoi, Yunheng Chen, Gyorgy Vizkelethy, Edward Bielejec, Marcus Doherty, Johannes Flick, and Carlos Meriles, in *Quantum 2.0 Conference and Exhibition* (Optica Publishing Group, 2022), p. QTu4A.2.
[21] H. Pernegger, S. Roe, P. Weilhammer, V. Eremin, H. Frais-Kölbl, E. Griesmayer, H. Kagan, S. Schnetzer, R. Stone, W. Trischuk, D. Twitchen, and A. Whitehead, Charge-carrier properties in synthetic single-crystal diamond measured with the transient-current technique, J. Appl. Phys. **97**, 073704 (2005).
[22] S. Gkoumas, A. Lohstroh, and P. J. Sellin, Low temperature time of flight mobility measurements on synthetic single crystal diamond, Diam. Relat. Mater. **18**, 1338 (2009).
[23] L. S. Pan, D. R. Kania, P. Pianetta, J. W. Ager, M. I. Landstrass, and S. Han, Temperature dependent mobility in single-crystal and chemical vapor-deposited diamond, J. Appl. Phys. **73**, 2888 (1993).
[24] A. Alberigi Quaranta, C. Canali, and G. Ottaviani, A 40 keV pulsed electron accelerator, Rev. Sci. Instrum. **41**, 1205 (1970).
[25] W. Shockley, Currents to conductors induced by a moving point charge, J. Appl. Phys. **9**, 635 (1938).
[26] S. Ramo, Currents induced by electron motion, Proc. IRE **27**, 584 (1939).
[27] K. Konishi, I. Akimoto, J. Isberg, and N. Naka, Diffusion-related lifetime and quantum efficiency of excitons in diamond, Phys. Rev. B **102**, 195204 (2020).
[28] J. Pernot, P. N. Volpe, F. Omnès, P. Muret, V. Mortet, K. Haenen, and T. Teraji, Hall hole mobility in boron-doped homoepitaxial diamond, Phys. Rev. B **81**, 205203 (2010).
[29] Nobuko Naka, Katsuyuki Fukai, Yushi Handa, and Ikuko Akimoto, Direct measurement via cyclotron resonance of the carrier effective masses in pristine diamond, Phys. Rev. B **88**, 035205 (2013).
[30] Markus Gabrysch, Ph.D. thesis, Uppsala University (2011).
[31] J. Isberg, S. Majdi, M. Gabrysch, I. Friel, and R. S. Balmer, A lateral time-of-flight system for charge transport studies, Diam. Relat. Mater. **18**, 1163 (2009).
[32] S. Majdi, Ph.D. thesis, Uppsala University (2012).
[33] See Supplemental Material at http://link.aps.org/supplemental/10.1103/PhysRevApplied.20.024037 for the evaluation of the drift velocity errors. The Supplemental Material also contains Refs. [14,30,32,34].
[34] H. Spieler, Fast timing methods for semiconductor detectors, IEEE Trans. Nucl. Sci. **29**, 1142 (1982).
[35] D. M. Caughey and R. E. Thomas, Carrier mobilities in silicon empirically related to doping and field, Proc. IEEE **55**, 2192 (1967).
[36] See Supplemental Material at http://link.aps.org/supplemental/10.1103/PhysRevApplied.20.024037 for the fitting method and uncertainties in the evaluation of the low-field mobility errors.
[37] See Supplemental Material at http://link.aps.org/supplemental/10.1103/PhysRevApplied.20.024037 for the evaluation method of the light and heavy holes mobility values, relaxation times and mean free paths at 13K. The Supplemental Material also contains Ref. [16].
[38] Yoon Jang Chung, C. Wang, S. K. Singh, A. Gupta, K. W. Baldwin, K. W. West, R. Winkler, M. Shayegan, and L. N. Pfeiffer, Record-quality GaAs two-dimensional hole systems, Phys. Rev. Mater. **6**, 034005 (2022).
[39] Luca Banszerus, Michael Schmitz, Stephan Engels, Matthias Goldsche, Kenji Watanabe, Takashi Taniguchi, Bernd Beschoten, and Christoph Stampfer, Ballistic transport exceeding 28 μm in CVD grown graphene, Nano Lett. **16**, 1387 (2016).